Geostationary Imaging FTS (GIFTS) Data Processing: Measurement Simulation and Compression

Hung-Lung Huang[a], H. E. Revercomb[a], J. Thom[a], P. B. Antonelli[a],
B. Osborne[a], D. Tobin[a], R. Knuteson[a], R. Garcia[a], S. Dutcher[a], J. Li[a] , and W. L. Smith[b]

[a]Space Science and Engineering Center, University of Wisconsin-Madison,
1225 W. Dayton Street, Madison, WI 53706
[b]NASA Langley Research Center, 100 NASA Road, Hampton, VA 23681-2199

ABSTRACT

GIFTS, a forerunner of next generation geostationary satellite weather observing systems, will be built to fly on the NASA EO-3 geostationary orbit mission in 2004 to demonstrate the use of large area detector arrays and readouts. Timely high spatial resolution images and quantitative soundings of clouds, water vapor, temperature, and pollutants of the atmosphere for weather prediction and air quality monitoring will be achieved. GIFTS is novel in terms of providing many scientific returns that traditionally can only be achieved by separate advanced imaging and sounding systems. GIFTS' ability to obtain half-hourly high vertical density wind over the full earth disk is revolutionary.

However, these new technologies bring forth many challenges for data transmission, archiving, and geophysical data processing. In this paper, we will focus on the aspect of data volume and downlink issues by conducting a GIFTS data compression experiment. We will discuss the scenario of using principal component analysis as a foundation for atmospheric data retrieval and compression of uncalibrated and un-normalized interferograms. The effects of compression on the degradation of the signal and noise reduction in interferogram and spectral domains will be highlighted. A simulation system developed to model the GIFTS instrument measurements is described in detail.

1. The Geostationary Imaging Fourier Transform Spectrometer

GIFTS uses a Michelson interferometer with two detector arrays, covering the spectral bands 685–1130 cm^{-1} and 1650–2250 cm^{-1} (Figure 1) to achieve vertical profiling of temperature and water.

Features of the GIFTS instrument relevant to this discussion can be summarized as: (a) using a large area format focal plane detector array (128 × 128 pixels) in a Fourier Transform Spectrometer (FTS)[1,2] mounted on a geostationary satellite; (b) simultaneous observation at high spectral (as great as 0.3 cm^{-1}) and spatial (4-km × 4-km pixel) resolution over a large area (512-km × 512-km) of the earth within a 10–20 second time interval, with selectable spectral resolution; (c) a visible low light level camera provides quasi-continuous imaging of clouds at 1-km spatial resolution; and (d) extended earth coverage is achieved by step scanning the instrument field of view in a contiguous fashion across any desired portion of the visible earth (Smith et al., 2000).

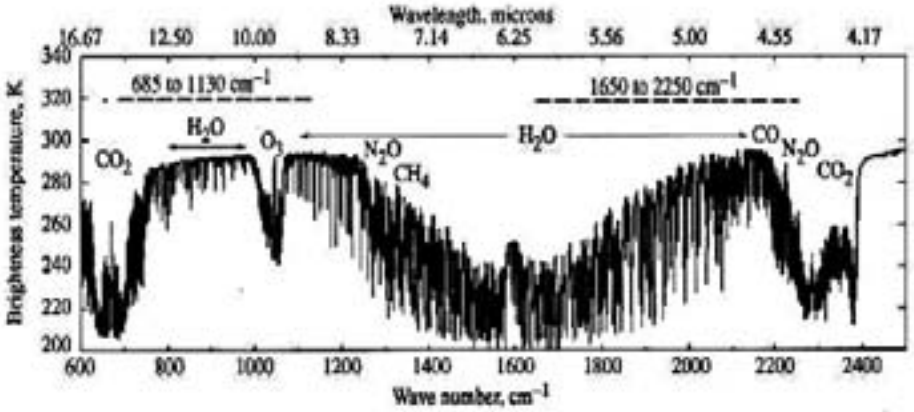

Figure 1. GIFTS spectral coverage (dashed lines), together with key spectral features of radiatively active atmospheric constituents.

2. GIFTS Measurement Simulation

The general methodology used to create the simulated GIFTS data cubes is to: (1) produce/obtain the simulated atmospheric state fields (meteorological profiles and clouds) for the GIFTS viewing scenario (described in Section 2.1), (2) calculate the top-of-atmosphere radiances from the atmospheric state (Section 2.2), and (3) apply the GIFTS specific instrumental effects to the incident radiances (Section 2.3). This last step includes the simulation of blackbody view data and noise. The following sections describe these three steps in detail.

2.1 Generation of Atmospheric State

This section describes the generation of atmospheric state and cloud parameters from UW-NMS. The University of Wisconsin Non-hydrostatic Modeling System (UW-NMS) is a model developed by Professor Greg Tripoli at UW-Madison. Input to the NMS model includes skin temperature, water vapor mixing ratio, ozone concentration, surface elevation, and liquid and ice water paths. A cloud-top height (set to the altitude at which the logarithm of the density of the cloud's liquid or ice content exceeds 0.25) is also input to the UW-NMS.

Some features of the UW-NMS model include:

- Arbitrary resolution in all directions
- Local spherical coordinate system in horizontal
- Height coordinate system with step topography using a terrain following variable grid spacing near the ground
- Multiple two-way interactive grid nesting, with moveable inner grids
- Gridscale microphysics parameterization with cloud water, rain, pristine crystals, snow, aggregate crystals, and graupel
- Modified Emanuel convective parameterization scheme
- Long/Short wave radiation parameterization with clouds
- Diffusion based on TKE prediction

Additional information on UW-NMS is available at http://mocha.meteor.wisc.edu/uw-nms.html.

2.2 UW GIFTS Fast Forward Model

The forward model takes atmospheric state parameters (such as temperature, water vapor and other gas concentrations, and clouds) and derives satellite-altitude radiances.

2.2.1 Clear Sky Transmittances

The clear sky fast model used at UW employs the PLOD regression[3] to line-by-line calculations obtained with LBLRTM[4] using HITRAN96[5]. The line-by-line transmittance data were mapped to the GIFTS spectral domain using a maximum optical path difference of 0.872448 cm, with an effective spectral resolution of □ 0.6 cm^{-1}, and apodized (Kaiser-Bessel[6]) prior to performing the regression analysis.

2.2.2 Cloud effects

Cloud effects are incorporated into the UW Fast Radiance Model via an optical thickness parameterization scheme developed by Dr. Yong Hu of NASA Langley Research Center:

$$OT_l = WP_l\left(C_0 r_{e,l}{}^{C_1} + C_2\right) \quad \text{(liquid cloud)} \qquad (1)$$

$$OT_i = WP_i\left(C_0 r_{e,i}{}^{C_1} + C_2\right) \quad \text{(ice cloud)} \qquad (2)$$

where C_0, C_1 and C_2 are parameterization coefficients, WP is the water path, and r_e is the effective radius of the cloud particle. Subscripts *l* and *i* denote liquid and ice cloud, respectively. The cloud transmittance is then

$$\tau_{cloud} = \exp\left(-OT\right) \qquad (3)$$

The total transmittence profile is obtained by multiplying the molecular transmittance profile by the cloud transmittance for all atmospheric levels at and below the cloud level..

2.2.3 Radiance/Brightness Temperature

The total atmospheric transmittance profile is then used with the atmospheric temperature profiles and surface properties to compute the top-of-atmosphere radiances using the radiative transfer equation. The surface is represented as a blackbody radiator (unit emissivity) with skin temperatures as given by the numerical model. At this point, the apodization is removed from the calculated radiances by dividing the interferogram of the apodized spectrum by the Kaiser Bessel function and then transforming the unapodized interferogram back to the spectral domain. This process produces top-of-atmosphere radiances with spectral resolution of that of an ideal (on-axis) FTS with a maximum optical path difference as given in Section 3. An example of simulated top of atmosphere brightness temperature over the continental USA is shown in Figure 2 below.

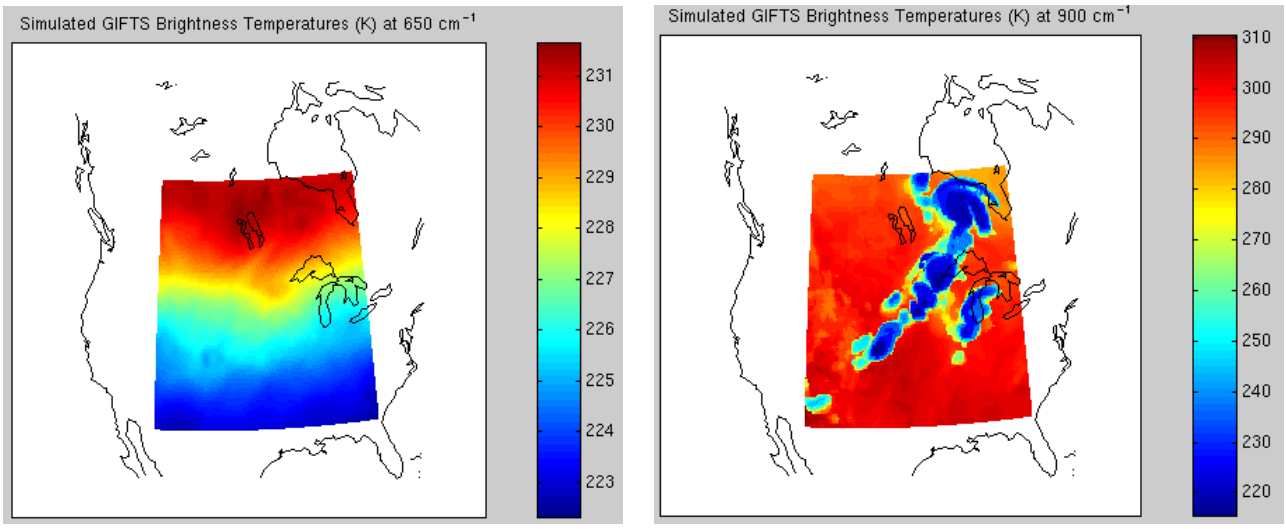

Figure 2. Top of atmosphere GIFTS brightness temperatures, in degrees Kelvin, at 650 and 900 cm^{-1}.

2.3 GIFTS Instrument Simulator

The Fourier Transform Spectrometer (FTS) instrument simulator models the significant instrumental effects of the GIFTS interferometer on the top-of-atmosphere simulated radiances. For each pixel in the GIFTS focal plane array (FPA), the FTS instrument simulator produces a simulated interferogram (or spectrum, if desired) of an Earth scene or calibration blackbody view. The instrumental effects modeled are: (1) addition of instrument background radiation, (2) application of the instrument responsivity magnitude and phase, (3) application of the numerical filter, (4) application of the instrument lineshape (ILS) function (self-apodization), and (5) the calculation, truncation and decimation of the interferogram. In this section we briefly discuss each of the simulator components in turn.

2.3.1 Instrument Background Radiation, $B_g(\nu)$

The radiation emitted from the optical assembly contributes to the signal measured by the instrument. In this version, only the emission from the telescope is included in the background radiation as shown below,

$$B_g(\nu) = \tau_t B(\nu, T_t) \qquad (4)$$

where τ_t and T_t are the emission and temperature of the telescope, respectively.

2.3.2 Instrument Responsivity, R_I

The instrument responsivity (or gain) is the function that relates incident radiance to observed counts. Ultimately the instrument responsivity will be determined as part of the on-board calibration process. For this simulation, the responsivity is assumed to have the spectral dependence from the combination of the detector property D^* and the interferometer modulation efficiency, MOD_EFF . Equation used to represent the responsivity is given as Equation 5,

$$R_I = (D^*)/(MOD\_EFF) \quad (5)$$

The calculation of responsivity is closely tied to the calculation of noise in order to provide a consistent simulation framework.

The instrument phase function $\varphi(\nu)$ is zero in this moment, leading to a symmetric interferogram.

2.3.3 Numerical Filter and Decimation, R_F

R_F is a representation of the GIFTS numerical filter. For now, the numerical filter is set to $R_F = 1.0$ within the GIFTS free spectral range and $R_F = 0$ outside this range. The decimation is set to provide 2048 points in the LW interferogram and 4096 points in the SW/MW interferogram. No attempt has been made to model a realistic numerical filter shape or to address quantization errors.

2.3.4 Simulation of GIFTS Self-apodization Effects

Both finite detector size and the presence of off-axis FTS paths in the GIFTS design produce self-apodization effects which act to distort the measured interferograms. For any FTS, if the on-axis optical path difference is d, then the optical path difference for a ray which passes through the interferometer at an angle θ from the optical axis is $d\cos(\theta)$. That is, all off-axis rays experience a slightly shorter optical path difference than the on-axis pathsThe off-axis effects are therefore characterized by a change in the optical path differences and by a reduction in spectral resolution due to modulation by the sinc function. The effects have a physical interpretation: the change in optical path difference is due to a non-zero central off-axis angle and the sinc function modulation is due to the integration over the solid angle associated with the finite detector size and the corresponding spread of interferogram sampling positions.

To simulate the off-axis wavenumber shift effects, an oversampled version of the input on-axis interferogram is produced. For a given pixel location, the central off-axis angle and the interferogram sampling interval, is then calculated. The oversampled interferogram is then simply interpolated to the off-axis sampling points to produce the off-axis interferogram. The associated spectrum is computed by taking the Fourier transform of the interferogram and calculating its corresponding spectral ranges, sampling interval, and wavenumber grid. Figure 3 demonstrates the self-apodization effects on GIFTS 128 × 128 FOV interferogram images. Where at zero path difference (first point of the interferogram) self-apodization effects is zero and at point 750 (0.66 Optical Path Difference (OPD)) self-apodization due to off-axis effects is very strong.

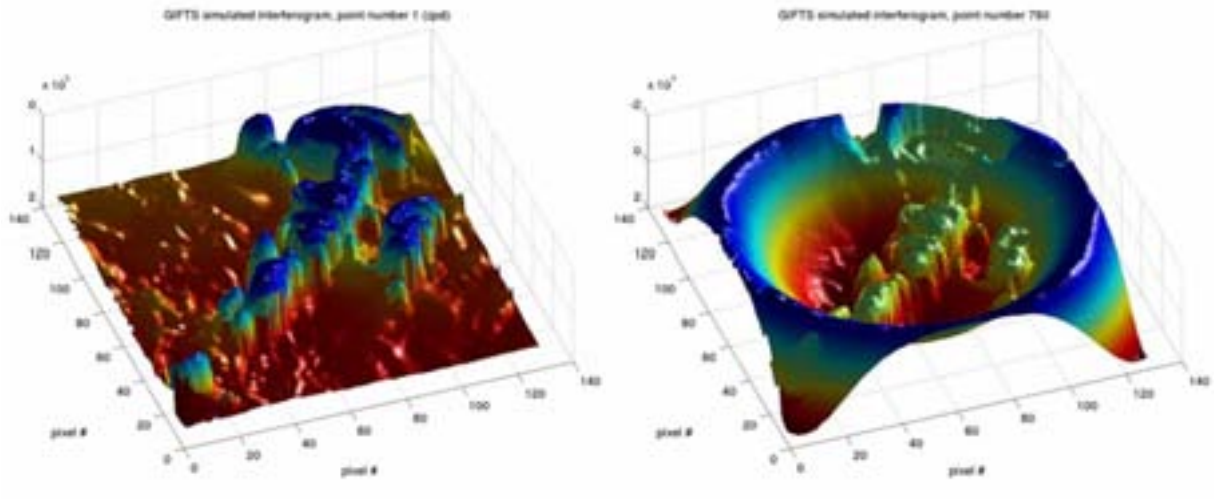

Figure 3. GIFTS interferogram data cubes at zero pass difference (ZPD) point (point 1 of interferogram) and point 750 (0.66 cm OPD). Self-apodization is non-existence at ZPD (left panel) and very dramatic at point 750. Frontal cloud feature is very pronounced from upper right to lower left corner.

2.3.5 Noise Simulation

The GIFTS instrument noise can be expressed as a noise equivalent spectral radiance, NESR, as

$$\mathrm{NESR}(\nu) = \frac{\mathrm{NESR}|_{\nu_r}}{D^*(\nu)} \times MOD\_EFF(\nu) \tag{6}$$

where $\mathrm{NESR}|_{\nu_r}$ is the noise level at reference wavenumber ν_r,

$$MOD\_EFF(\nu) = \left(\frac{1}{\varepsilon}\right)\left[1-(1-\varepsilon)\left(\frac{\nu}{\nu_r}\right)^2\right] \tag{7}$$

is the modulation efficiency,

$$D^*(\nu) = \left(\frac{\nu_r}{\nu}\right) f_{cut} \tag{8}$$

is the wavenumber-dependent part of the detector response, and the arbitrarily chosen cutoff function is chosen to provide a shape similar to detectors anticipated for GIFTS,

$$f_{cut} = \frac{\left[1-\exp\left(\frac{-(\nu-\nu_c)}{\nu_p}\right)\right]}{\left[1-\exp\left(\frac{-(\nu_r-\nu_c)}{\nu_p}\right)\right]} \tag{9}$$

Note that the detector noise is is assumed to be spectrally uncorrelated.

To produce the noise data cubes, the noise is first created in the uncalibrated interferogram domain. This is white noise (Gaussian distribution) in the double sided count interferogram domain. This noise is real and is not symmetric about the zero optical path difference. The amplitude (1 standard deviation) of this noise is such that the amplitude of the real part of the noise in the spectral count domain is $\mathrm{NESR} \times R_I$, which is equal to 1 count here. This requires the amplitude of this noise to be $\sqrt{2N}$ counts, where N is the number of points in the interferogram. The factor of $\sqrt{2}$ accounts for the complex nature of the spectral count noise and the $\sqrt{N}$ factor is due to the normalization of the inverse FFTs.

2.3.6 Simulated Calibration Blackbody-view Interferograms

Calibration blackbody interferograms generated for this simulation are represented as Planck radiances corresponding to brightness temperatures 2.726K (cosmic background), 250K (simulated telescope temperature), 265K (expected ambient blackbody temperature), and 300K (expected hot blackbody temperature) with unit emissivity.

3. GIFTS Measurement Compression Experiment

After analog to digital quantization, co-adding, hardware filter/decimation, bit trimming, and possible lossless compression, GIFTS will generate raw interferogram data at a rate of ~55 Mbps (megabytes per second). In order to keep the data stream volume to a reasonable level and the downlink affordable, the GIFTS project will conduct a Data Compression Experiment (DCE). Hardware to host the re-programmable DCE, yet to be identified, will be provided on board. Required features of the hardware include capability of performing vector processing with a minimum of a few GFLOPs and ability to read data from a high capacity, compact, low power memory at very high speeds. It will also be required to complete processing of the most recently collected data cube (128 × 128 FOVs) while the next scan is being collected. The goal of the data compression

experiment is to achieve a more desirable downlink data rate of 3–10 Mbps. This data rate is compatible with modest research and operational satellite telemetry systems. The GIFTS full raw data will also be downlinked to validate the compression experiment and will be used for further meteorological product generation and measurement validation.

3.1 Compression Algorithm Methodology

The baseline GIFTS compression algorithm is adapted from a well-known "Truncated Principal Component (TPC)[6]" concept used to compress interferogram and/or spectra, and retrieve sounding profiles. TPC is developed to compress measurements that filter out noise but preserve physical information content. TPC is applied to GIFTS measurements with the aim of providing 1) tolerable loss of interferogram or spectral information content, 2) noise reduction of each interferogram or spectral channel measurement, 3) a data compression effect with a compression ratio adequate for the GIFTS operational data downlink requirements, and 4) tolerable loss of accuracy in the profile retrieval. Other compression algorithms considered for GIFTS DCE, but not discussed in this paper, include imaging compression using codebooks and temporal feature preservation compression.

The noise reduction effect of TPC on the simulated noise is demonstrated in Figure 4, which compares the reconstructed noise using 10, 300, and 1000 principal components with the original noise. The first few significant principal components carry little information about the noise, while the higher order PCs carry more and more noise information. The signal information degradation and noise reduction as functions of the number of PCs used in the TPC compression is demonstrated in Figure 5. Using a suitable number of principal components for spectral compression can provide optimal compression that not only reduces noise but also preserves most of the physical information content.

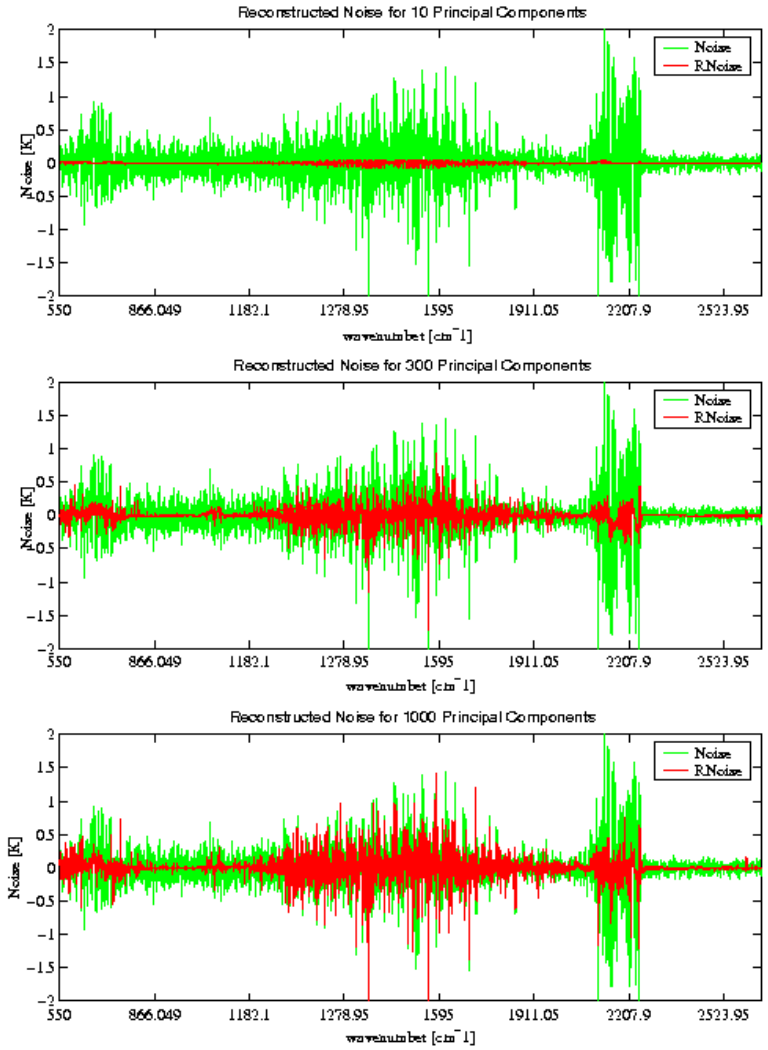

Figure 4. Noise (light hue) and compressed noise (dark hue).

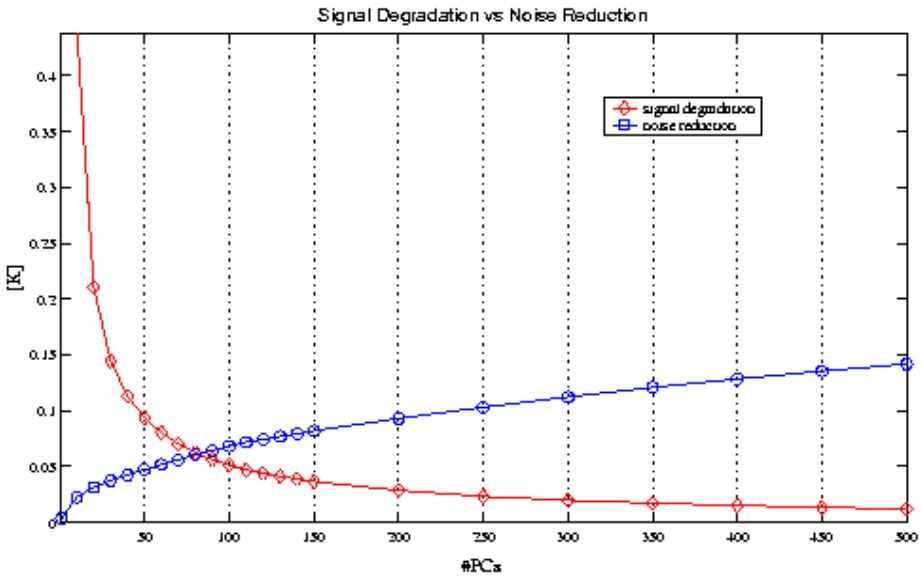

Figure 5. Signal degradation (diamonds) and noise reduction (circles) as a function of the number of principal components (PCs) used in the TPC.

3.2 Application of TPC to GIFTS Simulated Data

Simulated GIFTS data cubes (128 × 128 FOVs, with each 4 km FOV representing a longwave band interferogram with 2048 double sided points) are used to demonstrate the GIFTS compression algorithm that can account for 1) surface and atmospheric effects, 2) cloud effects, 3) off-axis effects produced by the focal plane array detector, and 4) uncalibrated measurements. An example of an uncalibrated single-sided GIFTS interferogram with off-axis effects is shown in Figure 6. At zero path difference (ZPD), the signal has maximum count value (extending past Figure 6's y-axis limits) and there is a second maximum at the first resonance region (centered near an optical path difference (OPD) of 0.66 cm, where strong CO_2 absorption contributes to the signal). For atmospheric temperature profile information, the two OPD regions of 0–0.1 cm and 0.6–0.7 cm contain most of the information content and any compression algorithm needs to preserve the information in these regions in particular.

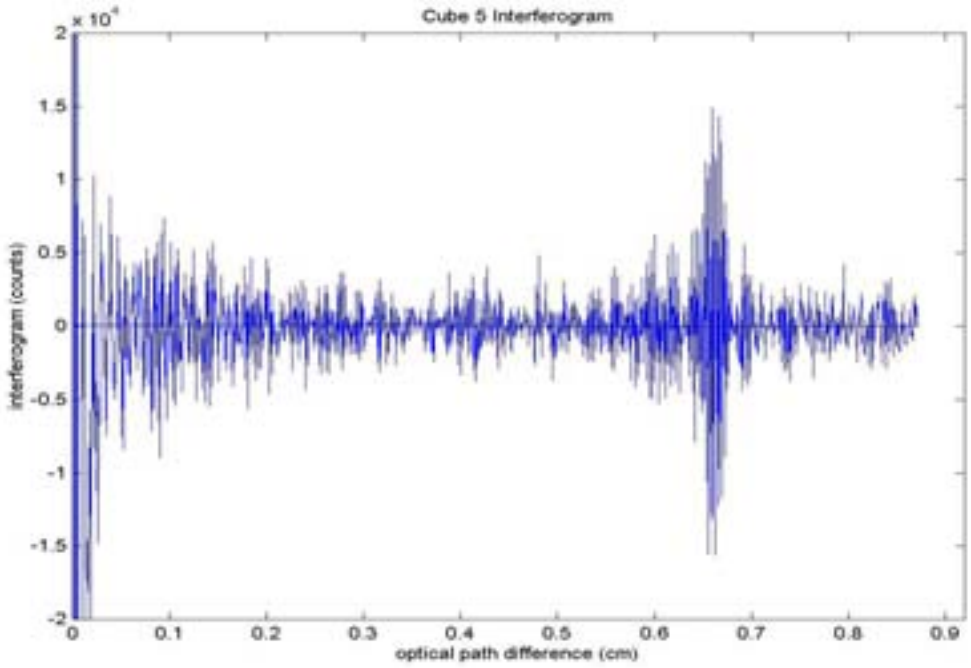

Figure 6. A sample GIFTS uncalibrated interferogram used in the data compression experiment.

Figure 7 and 8 show two simulated 128 × 128 GIFTS interferogram cubes at ZPD and point 780 (0.66 cm OPD), near the center of first resonance due to CO_2 absorption.

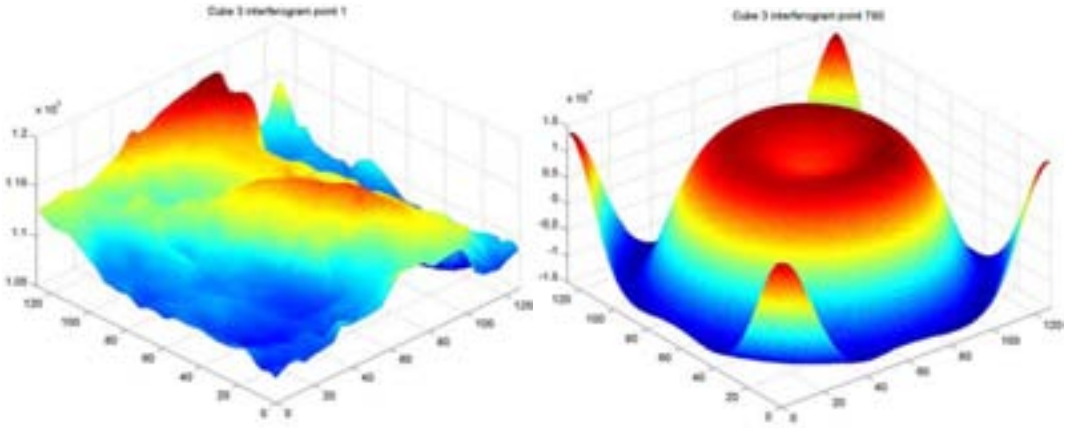

Figure 7. Cube 3 GIFTS interferogram image at ZDP (left) and 0.66 cm OPD (right).

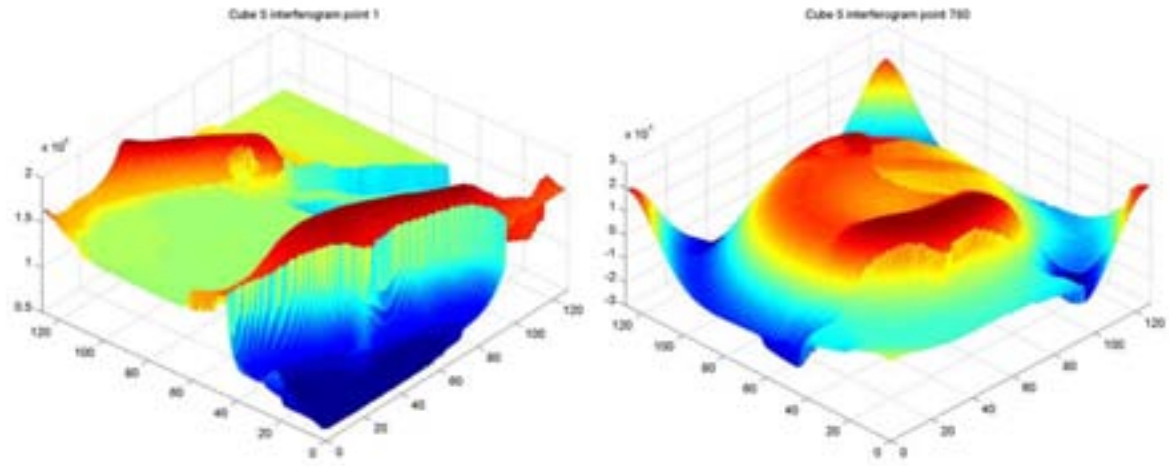

Figure 8. Cube 5 GIFTS interferogram image at ZDP (left) and 0.66 cm OPD (right)..

The wavy tails in four corners shown for the right hand panel of both Figures 7 and 8 are indications of detector array off-axis effects (as described in section 2.3.4). These off-axis effects generate additional signal variation on top of that from temperature and moisture variation in the scene, and create added challenges to the interferogram compression when off-axis effect is not accounted for a-priori. Figure 9 shows the Cube 2 point 780 (0.66 cm OPD) interferogram with and without off-axis effect. It can be seen that without off-axis effects, the CO_2 resonance signal has less variation which makes it potentially easier to achieve a higher compression ratio.

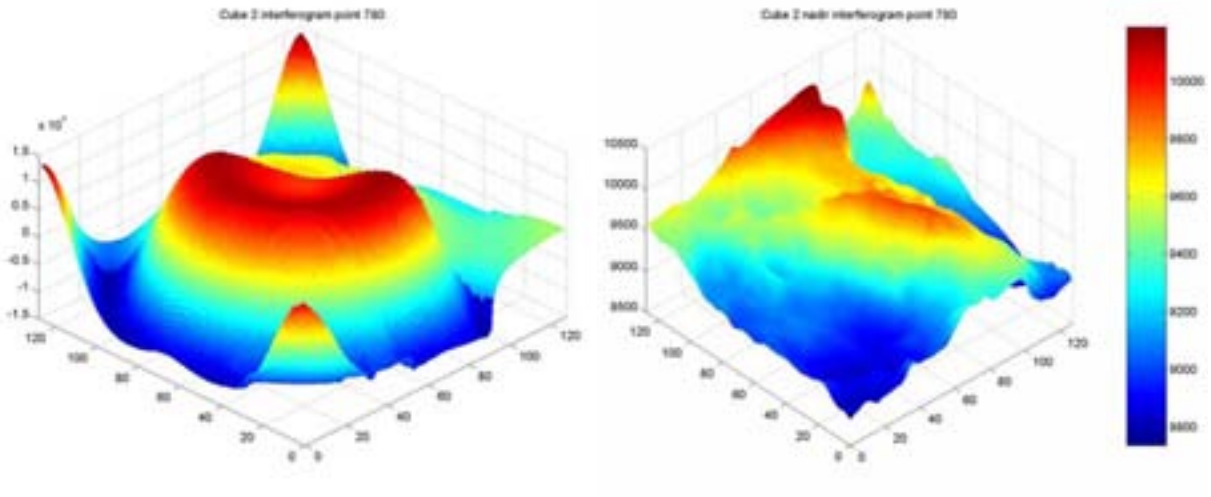

Figure 9. GIFTS first resonance interferogram image, with (left) and without (right) off-axis effect.

TPC compression is applied to each data cube using principal components derived from 41 interferograms selected from each individual cube. Each interferogram is broken down into 8 segments with 251 interferogram points each, leading to a 2048-point double sided simulated GIFTS interferogram for the IR longwave band. Forty near-ZPD points are not compressed. Figure 10 and 11 display the compression residual (root mean square error due to compression) and measurement noise in interferogram and spectral domains, respectively.

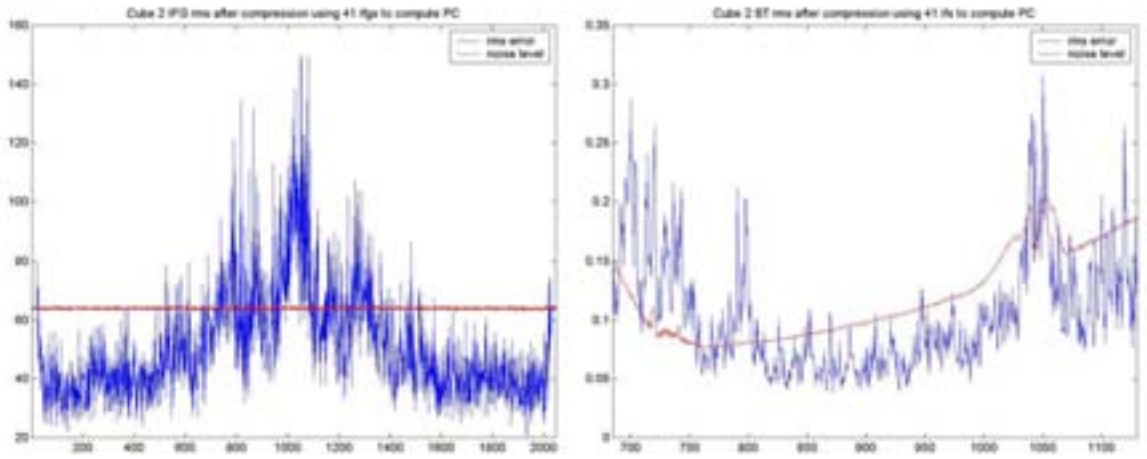

Figure 10. Cube 2 measurement noise (small variation) and compression residual (large variation) in the interferogram (left) and spectral domain (right).

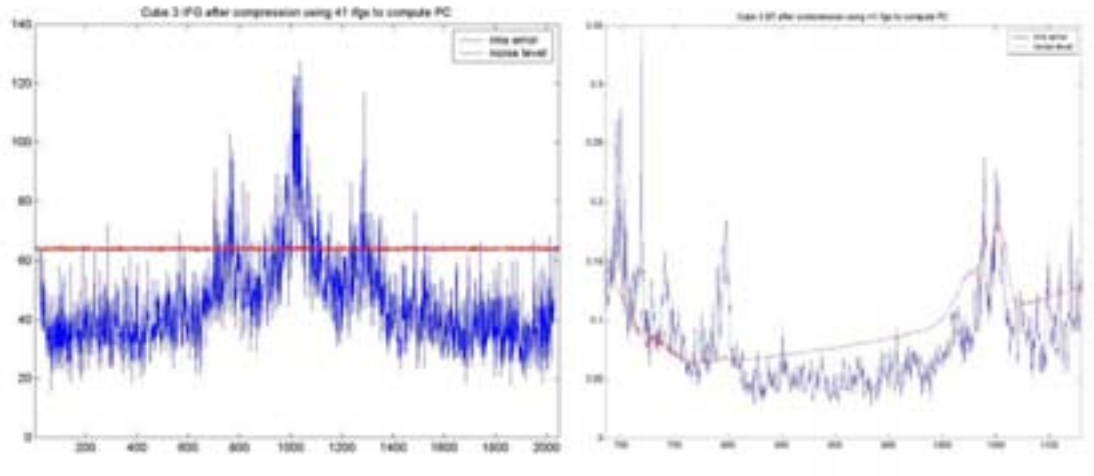

Figure 11. Cube 3 measurement noise (small variation) and compression residual (large variation) in the interferogram (left) and spectral domain (right).

The same compression procedure was used to compresses Cube 5 interferograms. The results show much higher compression residuals compared to the Cube 2 and 3 cases. To improve the compression, the number of interferograms selected for the derivation of PCs were increased from 41 to 547. The compression residuals in both interferogram and spectral domains are shown in Figure 12. These inconsistent compression results suggest that the current selection of sample interferograms for TPC is not optimal and further refinements are necessary.

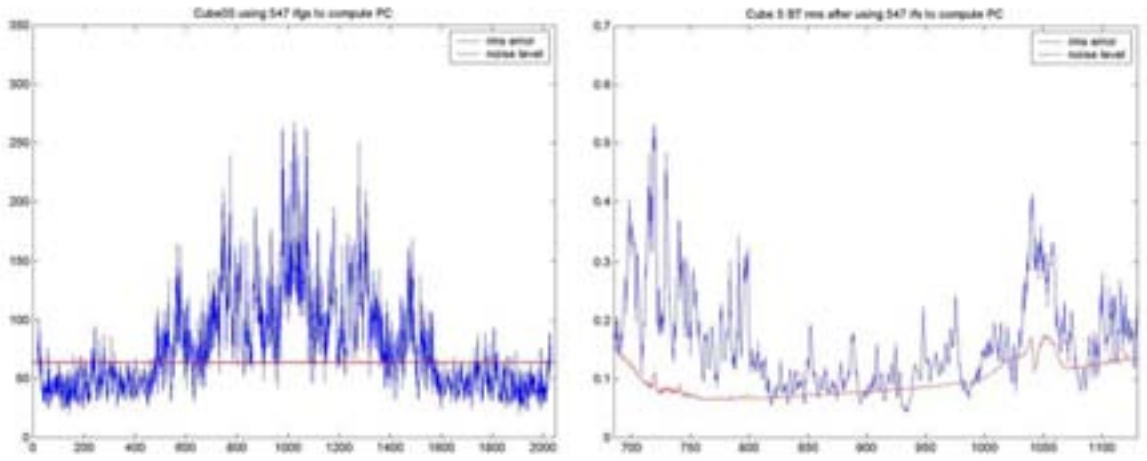

Figure 12. Cube 3 measurement noise (small variation) and compression residual (large variation) in the interferogram (left) and spectral domain (right).

The off-axis effect produces undesirable signal variation and affects the optimal compression outcome. Figure 13 shows the compression residual as if the cube 2 data had no off-axis effect (or off-axis effect can be accounted for perfectly).

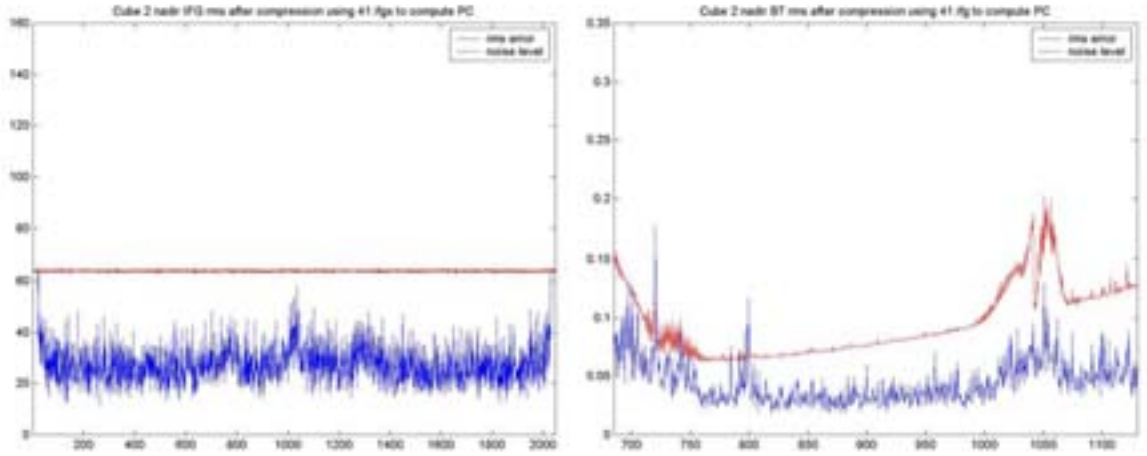

Figure 13. Measurement noise (small variation) and compression residual (large variation) for on-axis (i.e., no off-axis effect) cube 2 data in interferogram (left) and spectral (right) domain.

The compression outcomes due to the unique off-axis effect of the GIFTS detector array can be seen by comparing Figures 10 and 13. Without off-axis effects (Figure 13) the compression residual is fairly constant and always below noise level in the whole double sided interferogram. With off-axis effects, (Figure 10) the compression residual is larger than noise at regions near first resonance and near the maximum OPD, which translate residual error into most parts of the carbon dioxide and ozone absorption spectral regions. And larger than noise level residuals also exists near the 800 cm^{-1} region.

So far we have discussed the ongoing GIFTS compression algorithm experiment and results based on just a few cases of analysis. The current results are only preliminary and any firm conclusion should not be drawn from them. We are continuing to analyze more realistic and mature simulation measurements and refine algorithms to ensure GIFTS on-board and on-ground real time data processing system be available by the time GIFTS is in orbit.

4. Summary

GIFTS measurements are simulated from: (1) high spatial resolution (4 km) sounding profiles generated by a mesoscale numerical weather prediction model, 2) a radiative transfer model which accounts for cloud (ice and water cloud) effects, and 3) an instrument model of the background radiation, detector responsivity, self-apodization effects including off-axis variations, numerical filter and decimation effects, blackbody calibration, and noise. A baseline TPC compression algorithm developed for GIFTS data processing is outlined to demonstrate GIFTS technology and its measurement concept can be validated with efficient on-board and ground based data processing. The re-programmable nature of the compression algorithm will ensure future research and operational telemetry downlink is feasible and affordable. In particular, the TPC algorithm will be developed to meet the demanding real time process that requires only limited processing power. Tracking of these high-temporal resolution soundings in real time, not discussed in this paper, will lead to derived four-dimensional wind fields and ultimately demonstrate the revolutionary information that can be provided by GIFTS.

5. References

[1] Smith, W. L., H. B. Howell, and H. M. Woolf, 1979: The use of interferometric radiance measurements for sounding the atmosphere. *J. Atmos. Sci*., **36**, 566–575.

[2] Smith, W. L., H. E. Revercomb, D. D. LaPorte, L. A. Sromovsky, S. Silverman, H. M. Woolf, H. B. Howell, R. O. Knuteson, and H.-L. Huang, 1990: GHIS—The GOES High resolution Interferometer Sounder. *J. Appl. Meteor*., **29**, 1189–1204.

[3]S. Hannon, L. L. Strow, and W. W. McMillan, "Atmospheric infrared fast transmittance models: A comparison of two approaches," in *Proceedings of SPIE Conference 2830, Optical Spectroscopic Techniques and Instrumentation for Atmospheric and Space Research II* (12pp.), 1996

[4]S. A. Clough and M. J. Iacono, "Line-by-line calculations of atmospheric fluxes and cooling rates. 2: Applications to carbon dioxide, ozone, methane, nitrous oxide and the halocarbons." *J. Geophys. Res*., **100**, 16519–16535, 1995

[5]L. S. Rothman, R. R. Gamache, R. H. Tipping, C. P. Rinsland, M. A. H. Smith, D. C. Benner, V. Molathy Devi, J-M. Flaud, C. Camy-Peyret, A. Perrin, A. Goldman, S. Massie, L. R. Brown, and R. A. Toth, "The HITRAN Molecular Database: Editions of 1991 and 1992," *Journal of Quantitative Spectroscopy and Radiative Transfer* **48**, 469–507, 1992.

[6]H-L. Huang, and P. Antonelli, “Application of Principal Component Analysis to high resolution infrared measurement compression and retrieval”. Accepted by *J. Appl. Meteor.* for publication.

Smith, W. L., D. K. Zhou, F. W. Harrison, H. E. Revercomb, A. M. Larar, A. H. Huang, B. Huang, "Hyperspectral remote sensing of atmospheric profiles from satellites and aircraft", presented at SPIE's Second International Asia-Pacific Symposium on Remote Sensing of the Atmosphere, Environment, and Space, Sendai, Japan, 9–12 October 2000.